UNSUPERVISED NEURONAL MATCHING WITH SPONTANEOUS NEURONAL ACTIVITY

Anonymous authors
Paper under double-blind review

ABSTRACT

To obtain deeper understandings of the brain, aligning similarly functioning neurons, or matching neurons, in different neural systems is becoming an important problem in neuroscience. A major approach for neuronal matching is stimulus-based approach, where matching is performed through similarity of neuronal activity when exerted the same stimulation. This approach, however, is experimentally time-consuming and laborious, and we are in want for a more widely applicable matching approach that possibly uses more accessible data, such as spontaneous neural activity. Here we propose a neuronal matching framework that uses the spontaneous activity. The proposed method is based on an extension of Gromov-Wasserstein optimal transport (GWOT) (Mémoli, 2011b), which we named Gromov-Wasserstein optimal transport with multiple distance matrices (GWOT-MD). As a test of efficacy of the proposed approach, we applied the proposed framework to calcium imaging time series of spontaneous neuronal activities of *Caenorhabditis elegans* (*C.elegans*). Ratios of matching with pre-identified labels between individual pairs turned out much better than chance level matching ratios. We also performed neuron label identification using the matching results and revealed that the top 5 identification accuracy turned out as good as an identification method using neuronal locations (Sprague et al., 2024).

1 INTRODUCTION

Neuroscience has revealed various knowledge about the brain through comparison —i.e., identifying common or distinct features —of different neural systems. A crucial preliminary step in this comparative process is to align, or *match*, neurons that work similarly in different brains. Matching neurons provides accurate understandings of how similarly or differently the corresponding neurons act in different systems, helping detect individual differences (Kanai & Rees, 2011; Miller et al., 2012; Foulkes & Blakemore, 2018) or abnormalities in diseases (Wilson et al., 2023). Matching is necessary to control the neural systems via direct stimulation into neurons, e.g., optogenetics (Emiliani et al., 2022), as finding corresponding neurons would help reproducing functionally equivalent activity patterns in different systems (Muldoon et al., 2017; Kamiya et al., 2023). With the recent rapid developments of experimental techniques that allow spatially or temporally precise measurement (Ota et al., 2022) and control of neurons (Emiliani et al., 2022; Kravitz et al., 2010; Liu et al., 2020), elaborating neuronal matching frameworks is becoming a problem of practical significance in neuroscience rather than purely theoretical importance.

Existing neuronal matching methods can be divided into two major approaches —matching methods that use neural activity (Fig. 1(b,c)) and ones that use image-based information without neural activity (Fig. 1(a)). In the image-based approach, matching is performed based on similarities of neuronal morphology, locations, and gene expression patterns obtained as fluorescent colors (Yemini et al., 2021). Despite having seen massive success in neuronal matching in *Caenorhabditis elegans* (*C.elegans*) roundworms (Sprague et al., 2024; Nejatbakhsh & Varol, 2021; Varol et al., 2020; Chaudhary et al., 2021; Bubnis et al., 2019; Skuhersky et al., 2022; Toyoshima et al., 2020; Emmons et al., 2021) and *Drosophila* fruit flies (Peng et al., 2011; Zhao & Plaza, 2014; Veling et al., 2019), this approach in principle is limited in use to animals that have stereotypy across individuals, i.e., neuronal anatomy, lineage, and number are almost identical across individuals. Thus this approach cannot be applied to mammalian animals such as mice or human beings, where neuronal structures are much less stereotypical and far more complex. Furthermore, the neuronal identity de-

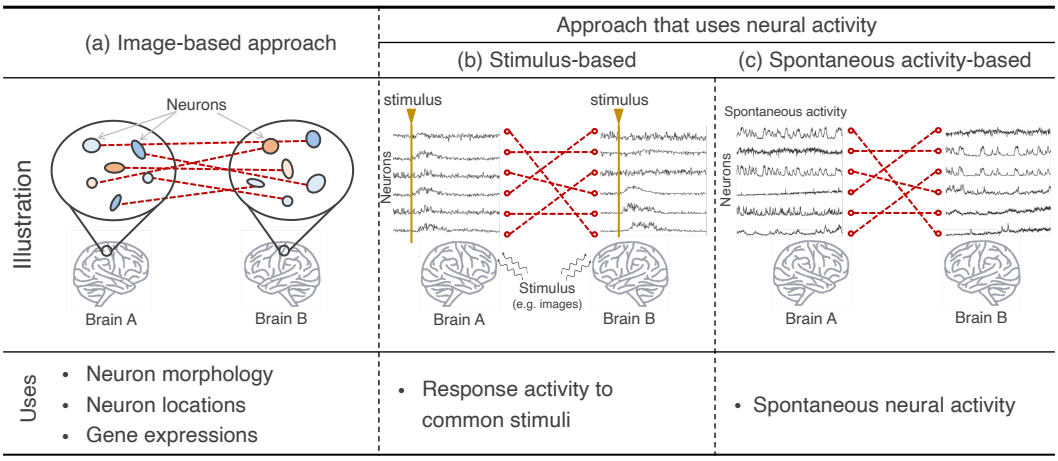

Figure 1: **Neuronal matching of neural systems.**

termined by anatomy or lineage does not always equate with neuronal functions (Guillermin et al., 2017; Rengarajan et al., 2019; Nakano et al., 2020; Sato et al., 2021), although many neurons seem to have consistent functions (Kato et al., 2015).

The other approach matches neurons based on similarity of neural activities. The most typical strategy is to use common stimuli (Fig. 1(b)) and match neurons according to the similarity of the responses to the same stimuli (Conroy et al., 2009; Haxby et al., 2011; Conroy et al., 2013; Thual et al., 2022). Despite its effectiveness, this strategy needs setting up experimental environments to exert common stimuli, making it laborious and time-consuming. In addition, matching is only based on only a finite number of stimulus responses, which covers a very small range of all neural representations (Luczak et al., 2009) and thus may provide a matching that does not generalize well to other stimuli.

While data using common controlled stimuli may be scarce due to experimental difficulties, a more accessible and abundant resource is spontaneous activity (Fig. 1(c)). Using spontaneous activity, neural activity engaging in no behavioral tasks or under no external stimulation, for neuronal matching would be a powerful and complementary method that provides additional information to stimulus-based matching. Spontaneous activity is most accessible, which saves experimentalists' cost and allows us to take data in abundance. Spontaneous activity is also known as ranging in broad representational spaces (Luczak et al., 2009), thus matching with spontaenous activity might generalize better than stimulus-based results.

There seems, however, no study of neuronal matching using spontaneous neural activity. This is apparently due to the difficulties that one faces in using spontaneous activity for matching purposes. Spontaneous activity does not have reference time points with which time series from different individuals are aligned, such as stimulus onsets, making it difficult to specify which parts of the signals should be compared. Thus, we must find another way than aligning time points to match neurons with spontaneous data.

In this work, we propose a novel neuronal matching framework that uses spontaneous neural activity (Fig. 1(c)). Instead of aligning timings, we aligned neurons grounded on the characteristics of a neuron relative to other neurons during the entire period of spontaneous activity. We made an assumption that neuron x in the brain A is functionally equivalent to neuron y in the brain B when the relationship between x and other neurons in A is equivalent to that between y and other neurons in B. This assumption is built upon the fact that there is a certain degree of commonality in the relational structures of neurons. (Susoy et al., 2021; Randi et al., 2023). We quantified this relationship of neurons with the (dis)similarity of spontaneous activity.

To obtain matching that preserves such relationship as similar as possible, we performed matching using Gromov-Wasserstein optimal transport (GWOT) (Mémoli, 2009), which is an unsupervised

matching method that tries to find the optimal mapping that preserves distance structures between systems as closely as possible.

Furthermore, to incorporate time delayed dissimilarity structures among neurons, we extend GWOT into what we named *Gromov-Wasserstein optimal transport with multiple distance matrices* (*GWOT-MD*). We made this extension as time delay structures in neural signals are pointed out to characterize spontaneous activity (Mitra et al., 2015), implying that considering time delay structures may contribute to better matching.

To test its efficacy, we applied GWOT-MD to spontaneous neural activity of *C.elegans*. We investigated how well our neuronal matching results coincide with the neuronal identities provided in datasets (Atanas et al., 2023; Kato et al., 2015; Uzel et al., 2022), relying on experimental evidence that the neurons of the same identity having relatively consistent functions (Kato et al., 2015; Susoy et al., 2021; Randi et al., 2023). We found that in matching between individual pairs, GWOT-MD showed matching ratios much better than chance level matching ratio. We also found incorporating time delay information contributed in improving matching ratios. To compare our matching results in previous studies (Sprague et al., 2024; Atanas et al., 2023; Varol et al., 2020; Chaudhary et al., 2021), we next examined how well we can estimate the neuron identity through the matching results of an individual to multiple individuals. The result turned out that the estimated accuracy was as good as information of neuronal locations, presenting that our framework can help specify neuronal identities in *C.elegans*.

Our contributions are:

- We proposed a framework for neuronal matching only using spontaneous neuronal activity.
- We proposed an extension of GWOT called GWOT-MD, which can incorporate time delay structures in matching.
- We applied our framework to *C.elegans* spontaneous neural activity and revealed a matching results comparable to locational information.

2 Background

Gromov-Wasserstein Optimal Transport

In this work, we utilize a mathematical framework called the Gromov-Wasserstein optimal transport, or GWOT for short (Mémoli, 2011b; Peyré et al., 2016), to find neuronal matching. GWOT, in short, aims to find the optimal way to transport a distribution to another distribution when we have only access to the distances between the points within the domain and the target distributions (Fig. 2).

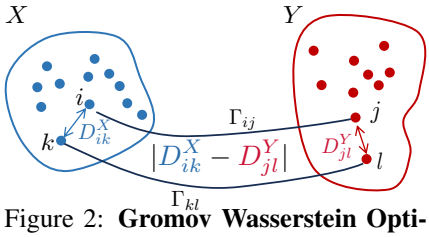

Figure 2: **Gromov Wasserstein Optimal Transport (GWOT).** The illustration is based on (Peyré et al., 2016).

Let us formulate GWOT in a more formal manner, following (Peyré et al., 2016) (Fig. 2). We summarized the notation that we used in Appendix A.

Problem 1 (GWOT) *Let X, Y be metric spaces equipped with distance d_X, resp., d_Y. We assume a discrete probability measure on each metric space is given as $\mu_p^X = \sum_{i=1}^m \delta_{x_i} p_i$ and $\mu_q^Y = \sum_{j=1}^n \delta_{y_j} q_j$, where $\{x_i\}_{i=1}^m \subset X$, $\{y_j\}_j^n \subset Y$, $p \in \Sigma_m$ and $q \in \Sigma_n$. GWOT problem is formulated as the next optimization problem:*

$$\mathrm{GW}(D^X, D^Y, p, q) := \min_{\Gamma \in \mathcal{C}_{p,q}} \mathcal{E}_{D^X, D^Y}(\Gamma), \tag{1}$$

$$\textit{where} \quad \mathcal{E}_{D^X, D^Y}(\Gamma) := \sum_{i,k} \sum_{j,\ell} L\left(D^X_{ik}, D^Y_{j\ell}\right) \Gamma_{ij} \Gamma_{k\ell}, \tag{2}$$

where $D^X_{ik} := d_X(x_i, x_k)$, $D^Y_{j\ell} := d_Y(y_j, y_\ell)$, $D^X = \{D^X_{ik}\}_{ik}$, $D^Y = \{D^Y_{j\ell}\}_{j\ell}$, and $L : \mathbb{R}_{\geqslant 0} \times \mathbb{R}_{\geqslant 0} \to \mathbb{R}_{\geqslant 0}$ is a measure of discrepancy between a pair of distances.

We set L as the quadratic loss $L(x, y) := \frac{1}{2}\|x-y\|^2$ as this is the most common choice (Peyré et al., 2016). We also note that we can rewrite the cost function (equation 2) as below,

$$\mathcal{E}_{D^X,D^Y}(\Gamma) = \left\langle \mathcal{L}(D^X, D^Y) \otimes \Gamma, \Gamma \right\rangle \tag{3}$$

where $\mathcal{L}(D^X, D^Y) = \left(L\left(D^X_{ik}, D^Y_{j\ell} \right) \right)_{ijk\ell}$.

The idea behind this minimization is as follows: consider a situation where one wants to transport a distribution whose histogram is given by $p = (p_1, \cdots, p_m)$ to another distribution with histogram $q = (q_1, \cdots, q_n)$ in a most effective manner. In this research, we only consider p and q to be uniform, described in Fig. 2 as the uniform size of dots. Unlike the normal *optimal transport* problem (Villani, 2009; Cuturi, 2013) where the cost of transporting p_i to q_j is pre-determined for each $(i, j) \in [\![m]\!] \times [\![n]\!]$, in GWOT we consider situations where the direct cost of transporting mass from p_i to q_j is not available, but only the distances of points within the same space are. Equation 2 tries to find $\Gamma \in \mathcal{C}_{p,q}$ such that the discrepancy among the distances with assignment or matching specified with Γ, whose ij element represents the weight that is carried from p_i to q_j, defined in each space becomes the smallest. Put in another way, GWOT problem searches for a transport plan Γ with which nearby points in X also come close in Y and vice versa and thus the distance structure is most well preserved. It is also known that equation 2 becomes a metric between the distributions p and q (Mémoli, 2009), offering a theoretical advantage of GWOT.

GWOT has been applied to many real-world systems to disclose correspondence or matching between two objects that are difficult to compare directly. Such GWOT applications include translation between two languages (Alvarez-Melis & Jaakkola, 2018), object matching (Mémoli, 2011a; Solomon et al., 2016), finding correspondence between two cell lineages (Demetci et al., 2022b;a), and aligning neural representations in brains (Kawakita et al., 2023; Takeda et al., 2024). The property of GWOT that spares any information of labels or correspondence in prior is called unsupervised property in some works (Kawakita et al., 2023; Sasaki et al., 2023), which makes GWOT an upcoming promising framework in neuroscience.

The computationally efficient solutions for GWOT have been proposed in several works (Peyré et al., 2016; Mishra et al., 2021; Ryner et al., 2023). Among these, the most well-known is the one proposed in Peyré et al. (2016), where equation 2 is iteratively optimized using Sinkhorn projection (Peyré & Cuturi, 2018).

3 Matching framework using spontaneous neural activity

3.1 Principles of Our Approach for Neuronal Matching

Here, we present our principle of neuronal matching. Our basic idea of matching with spontaneous neural activity is grounded on the relationship structure that neuronal population makes. That is, we assumed that neuron x in the brain A is functionally equivalent to neuron y in the brain B when the relationship between x and other neurons in A is equivalent to that between y and other neurons in B. This assumption is built upon fact that there is a certain degree of commonality in the relational structures of neurons across individuals of the same species (Susoy et al., 2021; Randi et al., 2023).

We quantified the relationship of neurons by the dissimilarity of spontaneous activity. As the dissimilarity measure, we adopted cosine distance $d_{\cos}$, one of the most frequent choices, between time series:

$$d_{\cos}(u, v) := 1 - \frac{{}^{\mathrm{t}}uv}{|u||v|} = 1 - \frac{u_1 v_1 + \cdots u_M v_M}{\sqrt{u_1^2 + \cdots + u_M^2}\sqrt{v_1^2 + \cdots + v_M^2}}. \tag{4}$$

Here, u and v describe a pair of spontaneous neural activities, $u = (u_1, \cdots, u_M)$, $v = (v_1, \cdots, v_M) \in \mathbb{R}^M$ $(M \in \mathbb{N})$.

Grounded on the assumption, what we seek is a matching that preserves the distance structures between a pair of individuals. As explained in the previous section, GWOT makes a nice path to this goal. We then proceed to use GWOT where the distances are the cosine distances defined above.

3.2 GWOT WITH MULTIPLE DISTANCE MATRICES (GWOT-MD)

In this section, we describe the novel matching method called GWOT-MD, an extension of GWOT. Although matching by GWOT seems a nice start for neuronal matching using spontaneous activity, it only matches dissimilarities between zero-lag activity, annihilating an important aspect of time series —time delayed relationships. Considering time delayed neuronal relationships or time dealayed functional connectivity well characterizes spontaneous activities (Mitra et al., 2015; Liégeois et al., 2017; Mitra et al., 2018), possibly improving extracting more precise functional relationships between neurons. We thus consider matching not only distances defined simultaneously but ones defined by some time delays. To do this, we extend GWOT to GWOT-MD to incorporate time delay structures, formulated as follows.

Problem 2 (GWOT-MD) *Let X, Y be metric spaces equipped with sets of distances $\{d_X^\tau\}_\tau$, resp., $\{d_Y^\tau\}_\tau$, each of which has the same finite number of elements. We set p, q, μ_p^X, μ_q^Y, as in Problem 1. GWOT-MT problem is formulated as the next optimization problem:*

$$\mathrm{GW}_{\mathrm{td}}(\{D^{X,\tau}\}, \{D^{Y,\tau}\}, p, q) := \min_{\Gamma \in \mathcal{C}_{p,q}} \mathcal{E}_{\{D^{X,\tau}\},\{D^{Y,\tau}\}}(\Gamma), \tag{5}$$

$$\textit{where} \quad \mathcal{E}_{\{D^{X,\tau}\},\{D^{Y,\tau}\}}(\Gamma) := \sum_{\tau=-h}^{h} \sum_{i,j,k,\ell} w_\tau L\left(D_{ik}^{X,\tau}, D_{j\ell}^{Y,\tau}\right) \Gamma_{ij}\Gamma_{k\ell}, \tag{6}$$

where $h \in \mathbb{N} \cup \{0\}$, $D_{ik}^{X,\tau} := d_X^\tau(x_i, x_k)$, $D_{j\ell}^{Y,\tau} := d_Y^\tau(y_j, y_\ell)$, $D^{X,\tau} = \{D_{ik}^{X,\tau}\}_{ik}$, $D^{Y,\tau} = \{D_{j\ell}^{Y,\tau}\}_{j\ell}$, and $L : \mathbb{R}_{\geqslant 0} \times \mathbb{R}_{\geqslant 0} \to \mathbb{R}_{\geqslant 0}$ is a measure of discrepancy between a pair of distances.

As seen by the cost function equation 6, the GWOT-MD problem tries to find a matching that makes each $D_{ik}^{X,\tau}$ and $D_{j\ell}^{Y,\tau}$ as close as possible. This forms an extension of GWOT, where matching is only done distances D_{ik}^X and $D_{j\ell}^Y$. GWOT-MD contains the original GWOT under $h = 0$ and $\{d_X^\tau\} = \{d_X\}, \{d_Y^\tau\} = \{d_Y\}$.

How can we solve GWOT-MD? GWOT-MD can be readily solved with a similar algorithm that we employ in GWOT. We sketch this algorithm; see Appendix B for more details. We rewrite the cost function defined in equation 6 as

$$\mathcal{E}_{\{D^{X,\tau}\},\{D^{Y,\tau}\}}(\Gamma) = \sum_{i,j,k,\ell} \left[\sum_{\tau=-h}^{h} w_\tau L\left(D_{ik}^{X,\tau}, D_{j\ell}^{Y,\tau}\right)\right] \Gamma_{ij}\Gamma_{k\ell} \tag{7}$$

$$= \left\langle \mathcal{L}_{\mathrm{td}}\left(\{D^{X,\tau}\}, \{D^{Y,\tau}\}\right) \otimes \Gamma, \Gamma \right\rangle, \tag{8}$$

where

$$\mathcal{L}_{\mathrm{td}}\left(\{D^{X,\tau}\}, \{D^{Y,\tau}\}\right) := \left(\sum_{\tau=-h}^{h} w_\tau L\left(D_{ik}^{X,\tau}, D_{j\ell}^{Y,\tau}\right)\right)_{ijk\ell}. \tag{9}$$

Considering that the form of the cost function (equation 8) is analogous to the one in equation 3, we notice that we only have to replace $\mathcal{L}(D^X, D^Y)$ to $\mathcal{L}_{\mathrm{td}}\left(\{D^{X,\tau}\}, \{D^{Y,\tau}\}\right)$ in the computation. This consequently indicates that we can inherit the solution algorithm of GWOT to solve GWOT-MD.

To apply GWOT-MD to spontaneous activity time series, we set d_X^τ and d_Y^τ as the distances defined between time points of difference τ. This application tries to match distances defined between various time delays as close as possible. The distance between time series delayed by τ can be defined in a similar manner to autocorrelation or autocovariance of a time series. That is, given $u = (u_1, \cdots, u_M), \quad v = (v_1, \cdots, v_M) \in \mathbb{R}^M$ $(M \in \mathbb{N})$, the time delayed cosine distance is defined as

$$d_{\cos}^\tau(u, v) := 1 - \frac{u_1 v_{1+\tau} + \cdots + u_{M-\tau} v_M}{\sqrt{u_1^2 + \cdots + u_{M-\tau}^2}\sqrt{v_{1+\tau}^2 + \cdots + v_M^2}}, \tag{10}$$

where the time delay $\tau \in \{0\} \cup [\![M-1]\!]$. As $\{d_X^\tau\}$ and $\{d_Y^\tau\}$ in Problem 2, we let $\{d_X^\tau\} = \{d_{\cos}^\tau\}_{\tau=-h}^h$ and $\{d_Y^\tau\} = \{d_{\cos}^\tau\}_{\tau=-h}^h$ with $h \in \mathbb{N}$. Technically, $d_{\cos}^\tau$ is not a metric in the mathematical sense, as the symmetry, $d_{\cos}^\tau(x, y) = d_{\cos}^\tau(y, x)$, does not generally hold. We, however, relaxed the condition of $\{d_X^\tau\}$ and $\{d_Y^\tau\}$ being distances in a strict sense, and substituted the values of $\{d_{\cos}^\tau\}_{\tau=-h}^h$ as computed from the time series data. We made a tentative choice for the weights $\{w_\tau\}_\tau$ and set $w_\tau = 1\ \forall\tau$.

Table 1: **The overview of *C.elegans* datasets.** In this study, we chose three datasets that include spontaneous neuronal activity under two different states: freely moving and immobilized. An individual in Uzel et al. (2022) was excluded from analysis because of its exceedingly large FPS (5.05 Hz). FPS = frames per second.

Dataset	State	n	Duration	FPS	# neurons	# labeled neurons
Atanas et al. (2023)	Freely moving	21	$\approx$ 16 min.	1.67 Hz	109-153	60-111
Kato et al. (2015)	Immobilized	5	$\approx$ 15 min.	2.80 - 3.07 Hz	109-135	31- 47
Uzel et al. (2022)	Immobilized	5	$\approx$ 15 min.	3.06 - 3.82 Hz	125-154	47- 58

4 Neuronal Matching of *C.elegans*

To test the efficacy of our approach, we next applied our method to calcium imaging data of *C.elegans* neurons. We chose *C.elegans* for the test animal due to the stereotypy in neural system, composed of 302 neurons with their own names in any individual White et al. (1986). Each of these 302 neurons has relatively fixed functions (Ann K. Corsi & Chalfie, 2005; Kato et al., 2015), although with some exceptions (Rengarajan et al., 2019; Nakano et al., 2020). As we seek for functional matching, we can use these labels as reference, or tentative ground truth, for estimated matching. Technically, not all neurons are identified in most openly available datasets (Atanas et al., 2023; Kato et al., 2015; Uzel et al., 2022), but 30-95% of the recorded neurons are identified via visual inspection by experts, which still work as reference for matching (see Table 1).

We used data from three different openly available datasets, whose details are available in Table 1. One of these datasets consists of recordings of freely moving individuals (Atanas et al., 2023); the other two datasets consist of recordings of immobilized individuals (Kato et al., 2015; Uzel et al., 2022). We excluded one immobilized individual in Uzel et al. (2022) from analysis because its exceedingly large value of FPS can be problematic in later analysis. We used the latter two datasets as one extended dataset to increase the number of pairs of immobilized individuals, because the number of immobilized individuals in each dataset was rather small ($n = 5$ and 5) compared to the freely moving individuals ($n = 21$). We note that, as can be seen from Table 1, the numbers of pre-identified neurons (or, *labeled* neurons hereafter) differ among individuals, and thus the numbers of neurons with common labels differ among individual pairs. Fig. C.1 shows the numbers of the neurons with common labels for each dataset.

4.1 Procedure and a Demonstrative Example of Matching

We applied our framework to the *C.elegans* calcium imaging data as illustrated in Fig. 3. For a pair of individuals (Fig. 3(a)), we first compute the simultaneous and time delayed cosine distances (equation 4, equation 10) using neural activity time series of recorded neurons in all individuals (Fig. 3(b)). Here as the time series, we used $\Delta F/F_0$ after applying the first-order Butterworth high-pass filter with 0.01Hz cutoff. We applied this filter because we had an increase in representational similarity analysis (RSA) scores (Kriegeskorte et al., 2008) performed prior to the matching procedure, but the analyses without the filtering showed very similar results with the slightest worsening. Then obtained distances are substituted in GWOT-MD (Fig. 3(c)).

We then obtained the optimizer matrix Γ^*, which we call the *matching matrix* hereafter (Fig. 3(d)). Γ^* represents the weights at which the neurons in the first individual are assigned to the neurons in the second. More specifically, Γ^*_{ij} represents the weight of neuron i in the first individual assigned to neuron j in the second. We show, as an example, the matching matrix Γ^* between two freely moving individuals in Fig. 3(d).

We then evaluated the matching matrix Γ^* by how much the matching result coincided with the pre-identified neuron labels. For visualization purposes, we ordered the rows and columns of Γ^* so that the neurons with common labels come at the top left in the same order (Fig. 3(d)). The submatrix consisting of the neurons with common labels is framed with the white square. Note that obtaining Γ^* itself does not necessitate neuron label information. If the matching results and pre-identified labels agree, the submatrix should look like the identity matrix. We can see the diagonal elements of the submatrix have high values and its non-diagonal elements are relatively sparse, showing the

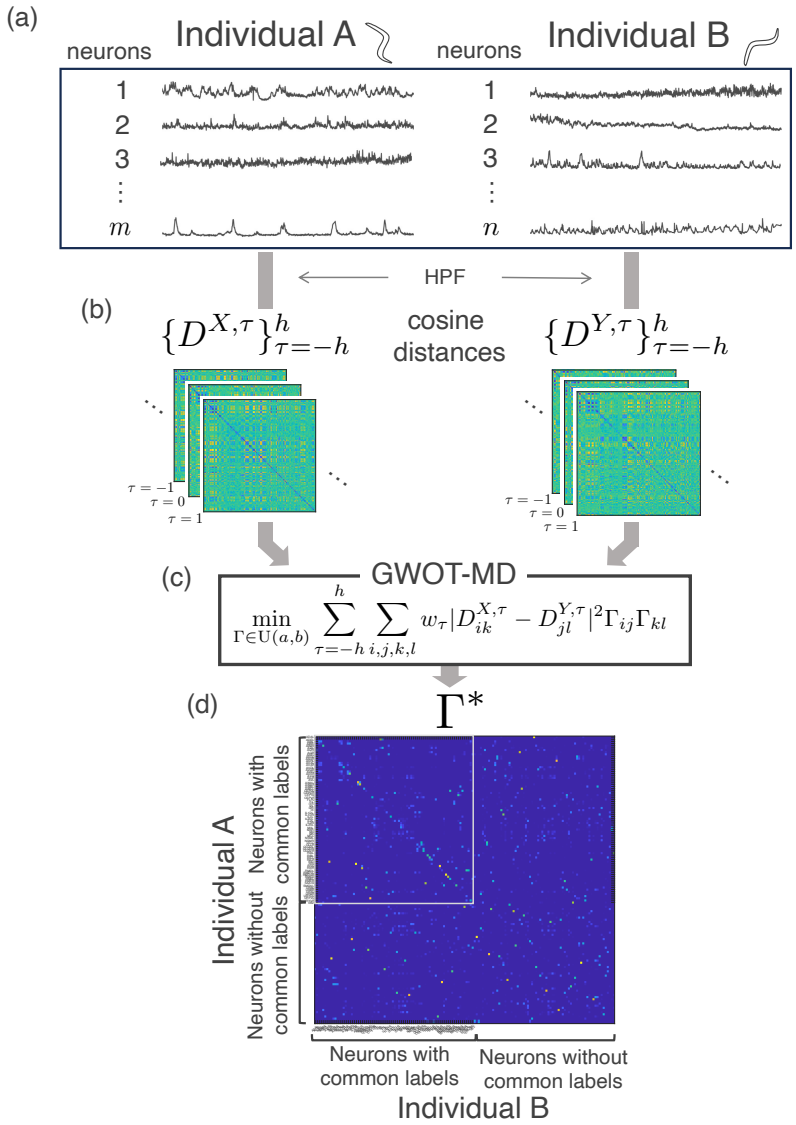

Figure 3: **Procedure of neuronal matching of *C.elegans*.** (a) We show an example using two individuals, A and B. The data are actual data of two individuals in (Atanas et al., 2023). (b) After applying a high pass filter, distance matrices (equation 10) are computed. (c,d) We solved GWOT-MD using these distance matrices to obtain the optimizer Γ^*, or the matching matrix. For ease of understandability, we rearranged the rows and columns in Γ^* so that the neurons with common labels in Individual A and B come to the left top (framed in white square) in the same lexicographical order. HPF = high pass filter.

similarity to the ground truth identity matrix. Therefore, in this specific example, the matching results and pre-identified labels seem to agree, despite a rather rough observation.

To quantitatively evaluate matching, using Γ^* we computed a measure that we call *top-k ratio*. This is a ratio of labeled neurons whose top-k matched neurons include the corresponding neuron in the other. We examined the ratio under three values of k: $k = 1, 5, 10$. See Fig. D.1 for a more specific and detailed explanation. We computed the top-k ratio of Γ^* of all pairs in each dataset.

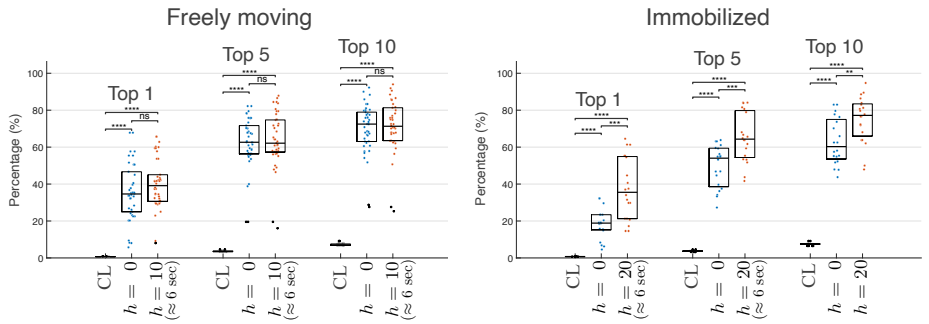

Figure 4: **Top-1, 5, and 10 matching ratios within the same individual, but between different time windows.** *Left: freely moving individuals*. Top-k matching ratios are plotted under $h = 0, 10$. Setting $h = 10$ amounts to 6 seconds in actual time. *Right: immobilized individuals*. Top-k matching ratios are plotted under $h = 0, 20$. Setting $h = 20$ amounts to 6 sec in actual time. To test if these increases were statistically significant, we utilized the Wilcoxon signed-rank test. CL = chance level.

4.2 Matching within the Same Individual between Different Time Windows

To determine the upper limit of neuronal matching across different worms, we first checked how the proposed matching results coincide with pre-identified neuron labels within the same individual in different but adjacent time windows. We performed the matching procedure in Fig. 3 within the same individual, regarding the first half and the second half of the time series data as different individuals. Assuming that there is little functional shift in neuron populations in an adjacent time window pair that is of $\simeq 10$ minutes length, the matching results of different individuals can not surpass the matching within the same individual. We describe our results of top-k ratios in Fig. 4 under $h = 0$ and under $h = 10$ in the freely moving individuals and $h = 20$ in the immobilized individuals[1]. We made an arbitrary choice of the values $h = 10$ and $h = 20$ so that the time intervals within which time delayed cosine distances (equation 10) were calculated became roughly the same (about 6 seconds). In the freely moving individuals, the top-k ratios were 34%, 63%, and 74% in top 1, top 5, and top 10 neurons, respectively, under $h = 0$. These values did not change significantly to 39%, 63%, and 70% under $h = 10$ (Fig. 4 (Left)). In the immobilized individuals, the top-k ratios were 20%, 54%, and 60% under $h = 0$. The values showed significant increase under $h = 20$, hitting 37%, 65%, and 78% (Fig. 4 (Right)). We can use these values as the references that settle the maxima of the extent to which the matching given by the proposed framework and the pre-identified labels agree.

4.3 Matching between Different Individuals

We examined to what extent neuronal matching coincide with neural labels between pairs of different individuals. In both the freely moving individuals and the immobilized individuals, we observed that the top-$1, 5,$, and 10 ratios become greater than the chance level values, indicated in CL (Fig. 5). In the freely moving individuals, the top-k ratios were 3%, 18%, and 27% in top 1, top 5, and top 10 neurons, respectively, under $h = 0$. The values showed significant increase under $h = 10$ and were 5%, 22%, and 30% (Fig. 5 (Left)). In the immobilized individuals, the top-k ratios were 5%, 25%, and 40% under $h = 0$. The values showed significant increase under $h = 20$ and were 12%, 38%, and 52% (Fig. 5 (Right)). These results show that incorporating time delays improved the matching to the pre-identified labels.

Here we chose h values arbitrarily, but the matching ratios reached plateau at $h = 10$ in freely moving individuals and $h = 20$ in immobilized ones, as shown in Figs. E.1 to E.6.

[1]Unlike the uniform FPS values in the freely moving individuals (1.67 Hz), the FPS values were different among the immobilized individuals ($2.80 - 3.82$ Hz). We, however, made no correction in FPS to compute time delayed cosine distances, as these FPS took mostly close values.

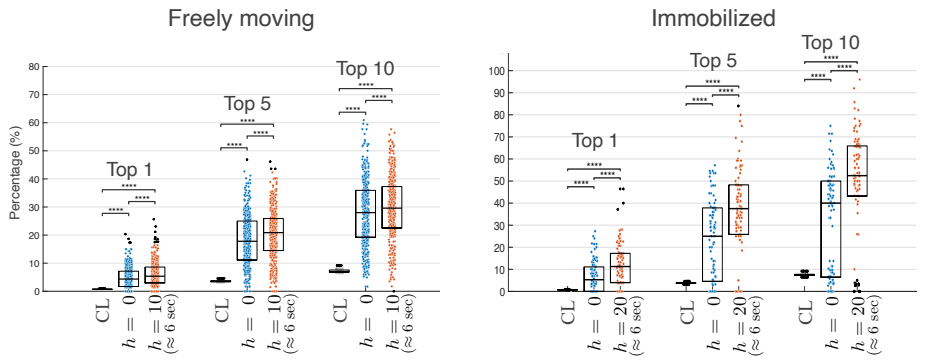

Figure 5: **Top-1, 5, and 10 matching ratios between different individuals.** *Left: freely moving individuals*. Top-k matching ratios of all 420 pairs (among 21 individuals) are plotted under $h = 0, 10$. Setting $h = 10$ amounts to 6 seconds in actual time. *Right: immobilized individuals*. Top-k matching ratios of all 90 pairs (among 10 individuals) are plotted under $h = 0, 20$. Setting $h = 20$ amounts to 6 sec in actual time. To test if these increases were statistically significant, we utilized the Wilcoxon signed-rank test. CL = chance level.

Table 2: **Top 5 identification accuracy by "majority vote" compared to previous results.** Median values of the top 5 accuracy are shown. The results of CPD (Coherent Point Drift) (Myronenko & Song, 2009), StatAtlas (Varol et al., 2020), and CRFID (Chaudhary et al., 2021) were based on Sprague et al. (2024). (direct comparison difficult)

		Methods in (Sprague et al., 2024)		
Method	GWOT-MD (ours)	CPD	StatAtlas	CRFID
Top 5 accuracy	**46%**	42%	64%	80%
Information	Spontaneous activity	Locations	Shapes & locations	Location & gene expression
# of training individuals	9	10	10	10

4.4 Neuron Label Identification Accuracy Compared to Previous Studies

To compare the matching performance with results in a previous study (Sprague et al., 2024), we next examined how well we can identify the label of neurons in individuals. To use our matching results for identification purpose, next performed what we call the "majority vote". In this majority vote, we estimated the label of a neuron in an individual by "voting" based on matching results with nine teacher worms whose labels were accessible. We tentatively allowed five votes for each teacher worm. See Appendix F for details.

We compared our results to ones in Sprague et al. (2024), where they performed automated neuronal identification using shapes, locations, and gene expressions. The matching accuracies in (Sprague et al., 2024), together with our result, are given in Table 2. In Sprague et al. (2024), three methods —CPD (Myronenko & Song, 2009), StatAtlas (Varol et al., 2020), and CRFID (Chaudhary et al., 2021) —were used for automated neuronal identification, and they utilize different information as shown in Table 2. In this table, we mixed our identification results in the freely moving and the immobilized individuals, as the results in (Sprague et al., 2024) were a mixture of several datasets of different locomotive states. We found that our result of 46% top 5 accuracy was better than CPD (42%), but worse than StatAtlas (64%) and CRFID (80%) (Table 2). Note that our results and the ones in (Sprague et al., 2024) in a strictly fair manner (where our model uses as training various combinations of 9 individuals in each dataset and each the model in (Sprague et al., 2024) uses as training 10 pre-determined worms). The accuracy of the proposed turned out as good as or slightly better that using locational information, but worse than those using locational, morphological, and genetic information.

5 Discussion

In this study, we proposed a novel method for neuronal matching using spontaneous neural activity. As spontaneous activity data is more accessible and abundant than data with stimuli, our matching method using spontaneous activity is can be a powerful complementary method to match functionally equivalent neurons. Also, matching estimated by spontaneous activity can generalize better than that estimated by stimulus-based method, since the neural activity ranges broader representational spaces Luczak et al. (2009). The proposed method is based on an optimization problem that we named GWOT-MD. We extended the normal GWOT to establish GWOT-MD to incorporate the dissimilarity structures among neurons of different time points. As a test of the efficacy of our approach, we applied the proposed framework to *C.elegans* calcium imaging data under the freely moving and immobilized states. We then computed the ratio of how much our matching result coincided with the neuron labels given in the dataset. As a result, the ratios turned much better than chance levels (Fig. 5). We also compared our results to previous image-based for neuron label identification, which turned out to be as good as the top 5 identification accuracy using information of neuronal locations.

Although we evaluated the matching results using pre-identified labels in the datasets, this evaluation may not be the best way to evaluate functional matching. This is because even for the identical neurons, their functions are reported to differ depending on time or individuals (Guillermin et al., 2017; Rengarajan et al., 2019; Nakano et al., 2020; Sato et al., 2021). We still consider that the pre-identified labels guarantees equity in functions to some extent (Susoy et al., 2021; Randi et al., 2023). How we can evaluate the goodness of functional matching is a difficult question, and we are under search of the better way to test functional matching. One possible way could be, for a given pair, to train a matching matrix using only a part of time series, and check if the similarity of the series increased after the obtained matching. We are to perform this analysis as a future analysis.

The matching ratios using GWOT-MD showed larger values within the same individuals under the immobilized state (Fig. 4) and between different individuals under the freely moving and immobilized states (Fig. 5). These results possibly shows that GWOT-MD, where matching is done over certain time delays, succeeded in unearthing time delayed structures that are to some extent preserved across individuals. More study is needed in what circumstances GWOT-MD performs better, or worse, than GWOT.

On the majority vote result, the top 5 accuracy of our framework was comparable to the previous automated neuronal identification results (Sprague et al., 2024). We speculate that this fairly large value of identification accuracy attributes to the same neurons having similar relationships if averaged over many individuals. Our approach using solely the neuronal activity time series can work as a complementary method to identify neurons, which can be employed with the image-based methods in tandem. We also are to specify neurons that are more accurately identified than others, possibly telling which neurons have consistently preserved functions in spontaneous activity.

Data Availability

All data is openly available. The data of the freely moving individuals can be downloaded from WormWideWeb (`https://wormwideweb.org/`); the data of the immobilized individuals can be downloaded from Open Science Framework (`https://osf.io/a64uz/`).

References

David Alvarez-Melis and Tommi Jaakkola. Gromov-Wasserstein alignment of word embedding spaces. In Ellen Riloff, David Chiang, Julia Hockenmaier, and Jun'ichi Tsujii (eds.), *Proceedings of the 2018 Conference on Empirical Methods in Natural Language Processing*, pp. 1881–1890, Brussels, Belgium, October-November 2018. Association for Computational Linguistics. doi: 10.18653/v1/D18-1214. URL `https://aclanthology.org/D18-1214`.

Bruce Wightman Ann K. Corsi and Martin Chalfie. A transparent window into biology: A primer on caenorhabditis elegans. In *WormBook*. ed. The C. elegans Research Community, 2005.

Adam A Atanas, Jungsoo Kim, Ziyu Wang, Eric Bueno, Mccoy Becker, Di Kang, Jungyeon Park, Talya S Kramer, Flossie K Wan, Saba Baskoylu, Ugur Dag, Elpiniki Kalogeropoulou, Matthew A Gomes, Cassi Estrem, Netta Cohen, Vikash K Mansinghka, and Steven W Flavell. Brain-wide representations of behavior spanning multiple timescales and states in C. elegans. *Cell*, 186(19): 4134–4151.e31, September 2023.

Greg Bubnis, Steven Ban, Matthew D DiFranco, and Saul Kato. A probabilistic atlas for cell identification. *arXiv*, pp. 1903.09227, March 2019.

Shivesh Chaudhary, Sol Ah Lee, Yueyi Li, Dhaval S Patel, and Hang Lu. Graphical-model framework for automated annotation of cell identities in dense cellular images. *Elife*, 10:e60321, February 2021.

Bryan R Conroy, Benjamin D Singer, J Haxby, and P Ramadge. FMRI-based inter-subject cortical alignment using functional connectivity. *Neural Inf Process Syst*, 22:378–386, December 2009.

Bryan R Conroy, Benjamin D Singer, J Swaroop Guntupalli, Peter J Ramadge, and James V Haxby. Inter-subject alignment of human cortical anatomy using functional connectivity. *Neuroimage*, 81:400–411, November 2013.

Marco Cuturi. Sinkhorn distances: Lightspeed computation of optimal transport. In C.J. Burges, L. Bottou, M. Welling, Z. Ghahramani, and K.Q. Weinberger (eds.), *Advances in Neural Information Processing Systems*, volume 26. Curran Associates, Inc., 2013. URL https://proceedings.neurips.cc/paper_files/paper/2013/file/af21d0c97db2e27e13572cbf

Pınar Demetci, Rebecca Santorella, Björn Sandstede, and Ritambhara Singh. Unsupervised integration of single-cell multi-omics datasets with disproportionate cell-type representation. In *Research in Computational Molecular Biology*, pp. 3–19. Springer International Publishing, April 2022a.

Pinar Demetci, Rebecca Santorella, Björn Sandstede, William Stafford Noble, and Ritambhara Singh. SCOT: Single-cell multi-omics alignment with optimal transport. *J. Comput. Biol.*, 29 (1):3–18, January 2022b.

Valentina Emiliani, Emilia Entcheva, Rainer Hedrich, Peter Hegemann, Kai R Konrad, Christian Lüscher, Mathias Mahn, Zhuo-Hua Pan, Ruth R Sims, Johannes Vierock, and Ofer Yizhar. Optogenetics for light control of biological systems. *Nat. Rev. Methods Primers*, 2(1):1–25, July 2022.

Scott W Emmons, Eviatar Yemini, and Manuel Zimmer. Methods for analyzing neuronal structure and activity in caenorhabditis elegans. *Genetics*, 218(4):iyab072, August 2021.

L Foulkes and S Blakemore. Studying individual differences in human adolescent brain development. *Nat. Neurosci.*, 21:315–323, February 2018.

Manon L Guillermin, Mayra A Carrillo, and Elissa A Hallem. A single set of interneurons drives opposite behaviors in C. elegans. *Curr. Biol.*, 27(17):2630–2639.e6, September 2017.

James V Haxby, J Swaroop Guntupalli, Andrew C Connolly, Yaroslav O Halchenko, Bryan R Conroy, M Ida Gobbini, Michael Hanke, and Peter J Ramadge. A common, high-dimensional model of the representational space in human ventral temporal cortex. *Neuron*, 72(2):404–416, October 2011.

Shunsuke Kamiya, Genji Kawakita, Shuntaro Sasai, Jun Kitazono, and Masafumi Oizumi. Optimal control costs of brain state transitions in linear stochastic systems. *J. Neurosci.*, 43(2):270–281, January 2023.

R Kanai and G Rees. The structural basis of inter-individual differences in human behaviour and cognition. *Nat. Rev. Neurosci.*, 12:231–242, April 2011.

Saul Kato, Harris S Kaplan, Tina Schrödel, Susanne Skora, Theodore H Lindsay, Eviatar Yemini, Shawn Lockery, and Manuel Zimmer. Global brain dynamics embed the motor command sequence of caenorhabditis elegans. *Cell*, 163(3):656–669, October 2015.

Genji Kawakita, Ariel Zeleznikow-Johnston, Naotsugu Tsuchiya, and Masafumi Oizumi. Comparing color similarity structures between humans and LLMs via unsupervised alignment. *arXiv*, August 2023.

Alexxai V Kravitz, Benjamin S Freeze, Philip R L Parker, Kenneth Kay, Myo T Thwin, Karl Deisseroth, and Anatol C Kreitzer. Regulation of parkinsonian motor behaviours by optogenetic control of basal ganglia circuitry. *Nature*, 466(7306):622–626, July 2010.

Nikolaus Kriegeskorte, Marieke Mur, and Peter Bandettini. Representational similarity analysis - connecting the branches of systems neuroscience. *Front. Syst. Neurosci.*, 2:4, November 2008.

Raphaël Liégeois, Timothy O Laumann, Abraham Z Snyder, Juan Zhou, and B T Thomas Yeo. Interpreting temporal fluctuations in resting-state functional connectivity MRI. *Neuroimage*, 163: 437–455, December 2017.

Weijie Liu, Chao Zhang, Jiahao Xie, Zebang Shen, Hui Qian, and Nenggan Zheng. Partial gromov-wasserstein learning for partial graph matching. *ArXiv*, abs/2012.01252, December 2020.

Artur Luczak, Peter Barthó, and Kenneth D Harris. Spontaneous events outline the realm of possible sensory responses in neocortical populations. *Neuron*, 62(3):413–425, May 2009.

Facundo Mémoli. Spectral Gromov-Wasserstein distances for shape matching. In *2009 IEEE 12th International Conference on Computer Vision Workshops, ICCV Workshops*, pp. 256–263. IEEE, September 2009.

Facundo Mémoli. A spectral notion of gromov–wasserstein distance and related methods. *Appl. Comput. Harmon. Anal.*, 30(3):363–401, May 2011a.

Facundo Mémoli. Gromov–Wasserstein distances and the metric approach to object matching. *Found. Comut. Math.*, 11(4):417–487, August 2011b.

Michael B Miller, Christa-Lynn Donovan, Craig M Bennett, Elissa M Aminoff, and Richard E Mayer. Individual differences in cognitive style and strategy predict similarities in the patterns of brain activity between individuals. *Neuroimage*, 59(1):83–93, January 2012.

Bamdev Mishra, N T V Satyadev, Hiroyuki Kasai, and Pratik Jawanpuria. Manifold optimization for non-linear optimal transport problems. *arXiv*, pp. 2103.00902, March 2021.

Anish Mitra, Abraham Z Snyder, Tyler Blazey, and Marcus E Raichle. Lag threads organize the brain's intrinsic activity. *Proc. Natl. Acad. Sci. U. S. A.*, 112(17):E2235–44, April 2015.

Anish Mitra, Andrew Kraft, Patrick Wright, Benjamin Acland, Abraham Z Snyder, Zachary Rosenthal, Leah Czerniewski, Adam Bauer, Lawrence Snyder, Joseph Culver, Jin-Moo Lee, and Marcus E Raichle. Spontaneous infra-slow brain activity has unique spatiotemporal dynamics and laminar structure. *Neuron*, 98(2):297–305.e6, April 2018.

Sarah Feldt Muldoon, Fabio Pasqualetti, Shi Gu, Matthew Cieslak, Scott T Grafton, Jean M Vettel, and Danielle S Bassett. Stimulation-based control of dynamic brain networks, August 2017.

Andriy Myronenko and Xubo Song. Point-set registration: Coherent point drift. *arXiv*, pp. 0905.2635, May 2009.

Shunji Nakano, Muneki Ikeda, Yuki Tsukada, Xianfeng Fei, Takamasa Suzuki, Yusuke Niino, Rhea Ahluwalia, Ayana Sano, Rumi Kondo, Kunio Ihara, Atsushi Miyawaki, Koichi Hashimoto, Tetsuya Higashiyama, and Ikue Mori. Presynaptic MAST kinase controls opposing postsynaptic responses to convey stimulus valence in caenorhabditis elegans. *Proc. Natl. Acad. Sci. U. S. A.*, 117(3):1638–1647, January 2020.

Amin Nejatbakhsh and Erdem Varol. Neuron matching in C. elegans with robust approximate linear regression without correspondence. In *2021 IEEE Winter Conference on Applications of Computer Vision (WACV)*, pp. 2836–2845. IEEE, January 2021.

Keisuke Ota, Hiroyuki Uwamori, Takahiro Ode, and Masanori Murayama. Breaking trade-offs: Development of fast, high-resolution, wide-field two-photon microscopes to reveal the computational principles of the brain. *Neurosci. Res.*, 179:3–14, June 2022.

Hanchuan Peng, Phuong Chung, Fuhui Long, Lei Qu, Arnim Jenett, Andrew M Seeds, Eugene W Myers, and Julie H Simpson. BrainAligner: 3D registration atlases of drosophila brains. *Nat. Methods*, 8(6):493–500, June 2011.

Gabriel Peyré and Marco Cuturi. Computational optimal transport. *arXiv*, pp. 1803.00567, March 2018.

Gabriel Peyré, Marco Cuturi, and Justin Solomon. Gromov-wasserstein averaging of kernel and distance matrices. In Maria Florina Balcan and Kilian Q. Weinberger (eds.), *Proceedings of The 33rd International Conference on Machine Learning*, volume 48 of *Proceedings of Machine Learning Research*, pp. 2664–2672, New York, New York, USA, 20–22 Jun 2016. PMLR. URL `https://proceedings.mlr.press/v48/peyre16.html`.

Francesco Randi, Anuj K Sharma, Sophie Dvali, and Andrew M Leifer. Neural signal propagation atlas of caenorhabditis elegans. *Nature*, 623(7986):406–414, November 2023.

Sophie Rengarajan, Kristen A Yankura, Manon L Guillermin, Wendy Fung, and Elissa A Hallem. Feeding state sculpts a circuit for sensory valence in caenorhabditis elegans. *Proc. Natl. Acad. Sci. U. S. A.*, 116(5):1776–1781, January 2019.

Martin Ryner, Jan Kronqvist, and Johan Karlsson. Globally solving the gromov-wasserstein problem for point clouds in low dimensional euclidean spaces. *arXiv*, pp. 2307.09057, July 2023.

Masaru Sasaki, Ken Takeda, Kota Abe, and Masafumi Oizumi. Toolbox for gromov-wasserstein optimal transport: Application to unsupervised alignment in neuroscience. *bioRxiv*, pp. 2023.09.15.558038, September 2023.

Hirofumi Sato, Hirofumi Kunitomo, Xianfeng Fei, Koichi Hashimoto, and Yuichi Iino. Glutamate signaling from a single sensory neuron mediates experience-dependent bidirectional behavior in caenorhabditis elegans. *Cell Rep.*, 35(8):109177, May 2021.

Michael Skuhersky, Tailin Wu, Eviatar Yemini, Amin Nejatbakhsh, Edward Boyden, and Max Tegmark. Toward a more accurate 3D atlas of C. elegans neurons. *BMC Bioinformatics*, 23 (1):195, May 2022.

Justin Solomon, Gabriel Peyré, Vladimir G Kim, and Suvrit Sra. Entropic metric alignment for correspondence problems. *ACM Trans. Graph.*, 35(4):1–13, July 2016.

Daniel Y Sprague, Kevin Rusch, Raymond L Dunn, Jackson M Borchardt, Greg Bubnis, Grace C Chiu, Chentao Wen, Ryoga Suzuki, Shivesh Chaudhary, Benjamin Dichter, Ryan Ly, Shuichi Onami, Hang Lu, Kotaro Kimura, Eviatar I Yemini, and Saul Kato. Unifying community-wide whole-brain imaging datasets enables robust automated neuron identification and reveals determinants of neuron positioning in C. elegans. *bioRxiv*, pp. 591397, April 2024.

Vladislav Susoy, Wesley Hung, Daniel Witvliet, Joshua E Whitener, Min Wu, Core Francisco Park, Brett J Graham, Mei Zhen, Vivek Venkatachalam, and Aravinthan D T Samuel. Natural sensory context drives diverse brain-wide activity during C. elegans mating. *Cell*, 184(20):5122–5137.e17, September 2021.

Ken Takeda, Kota Abe, Jun Kitazono, and Masafumi Oizumi. Unsupervised alignment reveals structural commonalities and differences in neural representations of natural scenes across individuals and brain areas. *bioRxiv*, pp. 613792, September 2024.

Alexis Thual, Quang Huy Tran, Tatiana Zemskova, Nicolas Courty, Rémi Flamary, Stanislas Dehaene, and Bertrand Thirion. Aligning individual brains with fused unbalanced gromov wasserstein. *Adv. Neural Inf. Process. Syst.*, 35:21792–21804, December 2022.

Yu Toyoshima, Stephen Wu, Manami Kanamori, Hirofumi Sato, Moon Sun Jang, Suzu Oe, Yuko Murakami, Takayuki Teramoto, Chanhyun Park, Yuishi Iwasaki, Takeshi Ishihara, Ryo Yoshida, and Yuichi Iino. Neuron ID dataset facilitates neuronal annotation for whole-brain activity imaging of *C. elegans*. *BMC Biol.*, 18(1):30, March 2020.

Kerem Uzel, Saul Kato, and Manuel Zimmer. A set of hub neurons and non-local connectivity features support global brain dynamics in C. elegans. *Curr. Biol.*, 32(16):3443–3459.e8, August 2022.

Erdem Varol, Amin Nejatbakhsh, Ruoxi Sun, Gonzalo Mena, Eviatar Yemini, Oliver Hobert, and Liam Paninski. Statistical atlas of C. elegans neurons. In *Lecture Notes in Computer Science*, Lecture notes in computer science, pp. 119–129. Springer International Publishing, Cham, 2020.

Macy W Veling, Ye Li, Mike T Veling, Christopher Litts, Nigel Michki, Hao Liu, Bing Ye, and Dawen Cai. Identification of neuronal lineages in the drosophila peripheral nervous system with a "digital" multi-spectral lineage tracing system. *Cell Rep.*, 29(10):3303–3312.e3, December 2019.

Cedric Villani. *Optimal Transport: Old and New*. Grundlehren der mathematischen Wissenschaften. Springer, Berlin, Germany, December 2009.

J G White, E Southgate, J N Thomson, and S Brenner. The structure of the nervous system of the nematode caenorhabditis elegans. *Philos. Trans. R. Soc. Lond. B Biol. Sci.*, 314(1165):1–340, November 1986.

David M Wilson, 3rd, Mark R Cookson, Ludo Van Den Bosch, Henrik Zetterberg, David M Holtzman, and Ilse Dewachter. Hallmarks of neurodegenerative diseases. *Cell*, 186(4):693–714, February 2023.

Eviatar Yemini, Albert Lin, Amin Nejatbakhsh, Erdem Varol, Ruoxi Sun, Gonzalo E Mena, Aravinthan D T Samuel, Liam Paninski, Vivek Venkatachalam, and Oliver Hobert. NeuroPAL: A multicolor atlas for whole-brain neuronal identification in C. elegans. *Cell*, 184(1):272–288.e11, January 2021.

Ting Zhao and Stephen M Plaza. Automatic neuron type identification by neurite localization in the drosophila medulla. *arXiv [q-bio.NC]*, September 2014.

A NOTATION

The sets of all positive integers, real numbers, and non-negative real numbers are denoted by $\mathbb{N}, \mathbb{R}$, and $\mathbb{R}_{\geqslant 0}$, respectively. For a matrix A, its transpose is denoted by ${}^{\mathrm{t}}A$. For $N \in \mathbb{N}$, $\mathbb{1}_N := {}^{\mathrm{t}}(1, \cdots, 1) \in \mathbb{R}^N$, and $[\![N]\!] := \{1, \cdots, N\}$. The probability simplex of dimension $N \in \mathbb{N}$, denoted by Σ_N, is the set of all N-dimensional histograms, and thus $\Sigma_N := \left\{ {}^{\mathrm{t}}(a_1, \cdots, a_N) \in \mathbb{R}^N_{\geqslant 0};\ a_i \geqslant 0,\ a_1 + \cdots + a_N = 1 \right\}$. A *coupling* between $p \in \Sigma_m$ and $q \in \Sigma_n$ $(m, n \in \mathbb{N})$ is a m-by-n matrix whose row- and column-wise sums are p and q respectively, and thus represents a joint distribution whose marginal distributions are p and q. The set of all couplings between $p \in \Sigma_m$ and $q \in \Sigma_n$, denoted by $\mathcal{C}_{p,q}$, is given as

$$\mathcal{C}_{p,q} = \{\Gamma \in \mathbb{R}^{m \times n}_{\geqslant 0};\ \Gamma \mathbb{1}_n = p,\ {}^{\mathrm{t}}\Gamma \mathbb{1}_m = q\}. \tag{11}$$

The entropy for a matrix $G \in \mathbb{R}^{m \times n}_{\geqslant 0}$ is defined as $H(G) := -\sum_{i,j,\ G_{ij} > 0} G_{ij} \log G_{ij} - G_{ij}$. The discrete probability measure concentrated on x in a measurable space $(X, \mathcal{B})$ is denoted by δ_x; i.e., for $A \in \mathcal{B}$ $\delta_x(A) = 1$ whenever $x \in A$ and 0 otherwise. Similarly in Peyré et al. (2016), the tensor–matrix multiplication $\otimes : \mathbb{R}^{m \times n \times p \times q} \times \mathbb{R}^{p \times q} \ni (\mathcal{L}, T) \mapsto \mathcal{L} \otimes T \in \mathbb{R}^{m \times n}$ is defined as

$$\mathcal{L} \otimes T := \left(\sum_{k,l} \mathcal{L}_{ijkl} T_{kl} \right)_{ij}. \tag{12}$$

B SOLUTION FOR GWOT & GWOT-MD

Here we show how we implemented GWOT and GWOT-MD solution algorithms. We start by presenting a solution for the conventional GWOT. We employed the entropic regularization GWOT (Peyré et al., 2016), one of the most standard solutions for GWOT. In this framework, we consider the following entropy-regularized version of the cost function equation 2,

$$\mathrm{GW}^{\varepsilon}(D^X, D^Y, p, q) := \min_{\Gamma \in \mathcal{C}_{p,q}} \mathcal{E}_{D^X, D^Y}(\Gamma) - \varepsilon H(T). \tag{13}$$

An efficient algorithm for this regularized problem, shown in Algorithm 1, was proposed in Peyré et al. (2016). This offers an approximation to the original problem if ε is small enough. As can be seen, this algorithm is strikingly simple.

Algorithm 1 Solution for Entropic GWOT

Input: $D^X \in \mathbb{R}^{m \times m}_{\geqslant 0}, D^Y \in \mathbb{R}^{n \times n}_{\geqslant 0}, p \in \Sigma_m, q \in \Sigma_n$
Output: $\Gamma = \arg\min_{\Gamma \in \mathcal{C}(p,q)} \mathcal{E}_{D^X, D^Y}(\Gamma) - \varepsilon H(\Gamma)$
  Initialize:
    $\Gamma \in \mathcal{C}(p, q)$
  repeat
    $\Gamma \leftarrow \mathrm{Sinkhorn}(\mathcal{L}(D^X, D^Y) \otimes \Gamma, p, q)$
  until convergence

Above, we set a tensor $\mathcal{L} \in \mathbb{R}^{m \times n \times m \times n}$,

$$\mathcal{L}_{ijk\ell} := \frac{1}{2} |D^X_{ik} - D^Y_{j\ell}|^2, \tag{14}$$

and $\mathrm{Sinkhorn}(A, p, q)$ the Sinkhorn projection of $A \in \mathbb{R}^{m \times n}$ onto $\mathcal{C}(p, q)$. The computational steps become even faster with an efficient technique to compute $\mathcal{L}(D^X, D^Y) \otimes \Gamma$, which utilizes the decomposition

$$\mathcal{L}(D^X, D^Y) \otimes \Gamma = c_{D^X, D^Y} - D^X \Gamma\, {}^{\mathrm{t}}D^Y, \tag{15}$$

where $c_{D^X, D^Y} := \frac{1}{2} \left((D^X)^2 p\, {}^{\mathrm{t}}\mathbb{1}_n + \mathbb{1}_m\, {}^{\mathrm{t}}q\, {}^{\mathrm{t}}(D^Y)^2 \right)$ is independent of Γ (the sign "$\cdot^2$" represents element-wise square) (Peyré et al., 2016).

We next move on to explaining the solution algorithm for GWOT-MD (Problem 2). We take the same path as we did in GWOT and consider the next entropy-regularized GWOT-MD,

$$\mathrm{GW_{td}}^{\varepsilon}(\{D^{X,\tau}\},\{D^{Y,\tau}\},p,q) := \min_{\Gamma\in\mathcal{C}_{p,q}} \mathcal{E}_{\{D^{X,\tau}\},\{D^{Y,\tau}\}}(\Gamma) - \varepsilon H(\Gamma). \tag{16}$$

This problem can be solved by only substituting $\mathcal{L}_{ijk\ell} =$ instead of equation 14.

Algorithm 2 Solution for Entropic GWOT-MD

Input: $\left\{D^{X,\tau}\right\}_{\tau=-h}^{h} \in \left(\mathbb{R}_{\geqslant 0}^{m\times m}\right)^{2h+1}, \left\{D^{Y,\tau}\right\}_{\tau=-h}^{h} \in \left(\mathbb{R}_{\geqslant 0}^{n\times n}\right)^{2h+1},\ p\in\Sigma_m,\ q\in\Sigma_n$
Output: $\Gamma = \arg\min_{\Gamma\in\mathcal{C}(p,q)} \mathcal{E}_{\{D^{X,\tau}\},\{D^{Y,\tau}\}}(\Gamma) - \varepsilon H(\Gamma)$
  Initialize:
    $\Gamma \in \mathcal{C}(p,q)$
  repeat
    $\Gamma \leftarrow \mathrm{Sinkhorn}(\mathcal{L}_{\text{td}}\left(\{D^{X,\tau}\},\{D^{Y,\tau}\}\right)\otimes\Gamma, p, q)$.
  until convergence

The tensor–matrix product is computed, using equation 15, as

$$\left(\mathcal{L}_{\text{td}}\left(\{D^{X,\tau}\},\{D^{Y,\tau}\}\right)\otimes\Gamma\right)_{ij} = \sum_{k,\ell}\sum_{\tau=-h}^{h} w_\tau L\left(D_{ik}^{X,\tau}, D_{j\ell}^{Y,\tau}\right)\Gamma_{k\ell} \tag{17}$$

$$= \sum_{\tau=-h}^{h} w_\tau \sum_{k,\ell} \mathcal{L}(D^{X,\tau}, D^{Y,\tau})\otimes\Gamma \tag{18}$$

$$= \sum_{\tau=-h}^{h} w_\tau c_{D^{X,\tau},D^{Y,\tau}} - \sum_{\tau=-h}^{h} w_\tau D^{X,\tau}\Gamma^{\mathrm{t}} D^{Y,\tau}. \tag{19}$$

We lastly note that being a non-convex optimization problem, it is generally difficult to obtain the global minimum of the optimization problem (equation 5) in GWOT-MD. We tried to deal with this problem by taking multiple ε values and by taking multiple initial values for the iterations. We performed computation with 21 values of ε: $\varepsilon \in \{10^{-4}, 10^{-3.8}, \cdots, 10^{-0.2}, 1\}$. For each ε, we took 50 initial values. From the $21\times 50 = 1050$ values of Γ^* obtained, we finally chose Γ^* that minimize the original cost function (equation 8, equation 9,).

C NUMBERS OF NEURONS WITH COMMON LABELS

Here we summarize the numbers of neurons with common labels between all pairs.

Freely moving (Anatas et al, 2023)

	1	2	3	4	5	6	7	8	9	10	11	12	13	14	15	16	17	18	19	20	21
1	78	64	64	54	54	50	58	59	52	73	51	59	44	53	32	58	49	57	62	64	56
2	64	87	71	58	61	54	65	67	53	75	63	67	46	59	33	61	57	59	68	71	60
3	64	71	95	61	65	56	68	77	54	84	67	72	56	69	43	74	67	66	78	77	66
4	54	58	61	74	58	48	63	61	52	69	58	64	47	52	36	61	55	59	61	61	55
5	54	61	65	58	84	49	65	66	51	71	59	62	49	55	38	61	56	58	58	62	56
6	50	54	56	48	49	69	56	57	46	58	52	55	37	52	33	55	51	49	57	56	54
7	58	65	68	63	65	56	91	70	54	78	63	68	51	61	37	67	61	59	69	67	62
8	59	67	77	61	66	57	70	95	55	83	68	72	56	68	43	73	63	60	71	75	63
9	52	53	54	52	51	46	54	55	67	61	54	57	40	51	28	54	51	51	54	58	50
10	73	75	84	69	71	58	78	83	61	111	73	78	59	72	47	81	73	73	83	84	70
11	51	63	67	58	59	52	63	68	54	73	91	72	47	65	43	67	69	63	72	71	60
12	59	67	72	64	62	55	68	72	57	78	72	90	51	65	37	70	65	67	71	76	62
13	44	46	56	47	49	37	51	56	40	59	47	51	71	47	40	56	45	49	51	51	44
14	53	59	69	52	55	52	61	68	51	72	65	65	47	85	39	67	62	57	69	67	59
15	32	33	43	36	38	33	37	43	28	47	43	37	40	39	60	47	41	38	44	42	35
16	58	61	74	61	61	55	67	73	54	81	67	70	56	67	47	92	67	65	75	77	64
17	49	57	67	55	56	51	61	63	51	73	69	65	45	62	41	67	87	63	71	69	55
18	57	59	66	59	58	49	59	60	51	73	63	67	49	57	38	65	63	87	66	66	55
19	62	68	78	61	58	57	69	71	54	83	72	71	51	69	44	75	71	66	96	80	67
20	64	71	77	61	62	56	67	75	58	84	71	76	51	67	42	77	69	66	80	95	65
21	56	60	66	55	56	54	62	63	50	70	60	62	44	59	35	64	55	55	67	65	82

Immobilized (Kato et al 2015, Uzel et al 2022)

	1	2	3	4	5	6	7	8	9	10
1	38	35	25	31	27	29	25	26	25	29
2	35	44	29	35	31	31	26	29	24	30
3	25	29	32	28	28	26	23	25	20	27
4	31	35	28	47	28	33	29	28	26	30
5	27	31	28	28	31	27	25	26	21	27
6	29	31	26	33	27	58	48	44	44	44
7	25	26	23	29	25	48	54	41	40	38
8	26	29	25	28	26	44	41	48	37	38
9	25	24	20	26	21	44	40	37	47	35
10	29	30	27	30	27	44	38	38	35	47

Figure C.1: **Numbers of neurons with common labels between each pair in the datasets.**

D CALCULATION OF TOP-k RATIO

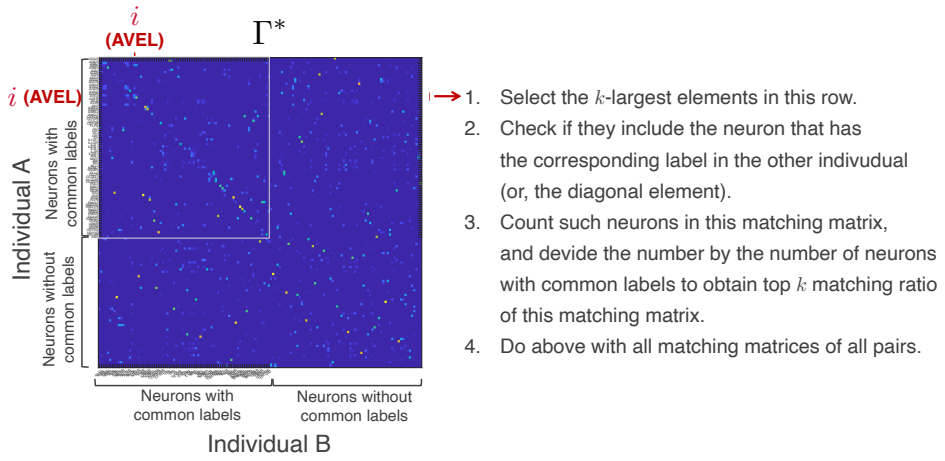

Figure D.1: **Demonstration of how to calculate the top-k ratio.** We here demonstrate using the same Γ^* as in Fig. 3 calculation of top-k matching ratio. We evaluated if matching coincides with the pre-identified labels using an index called the top-k matching ratio ($k = 1, 5, 10$). This index quantifies the ratio of neurons whose k-largest candidates in the matching matrix include the pre-identified label. The details are as follows. First, given a matching matrix between a pair (e.g., Individuals A and B as in Fig. 3), we fix a neuron (i) that has a common label (e.g., "AVEL") in the pair. Considering Γ^*_{ij} represents the weight of neuron i assigned to neuron j in the other, we examined if the k largest elements in the i'th row (i.e., $\{\Gamma_{ij}\}_j$) include the neuron with the same label ("AVEL"). In this figure, since the neurons with common labels are placed at the left top, one has to check if the k largest elements in the i'th row include the diagonal element. If this is the case, we call such a neuron a "good" neuron. We counted the number of "good" neurons and obtained the ratio of them by dividing the number of "good" neurons by the neurons with common labels. We repeated the same procedure with matching matrices of all pairs.

E MATCHING RESULTS WITH VARIOUS TIME DELAYS

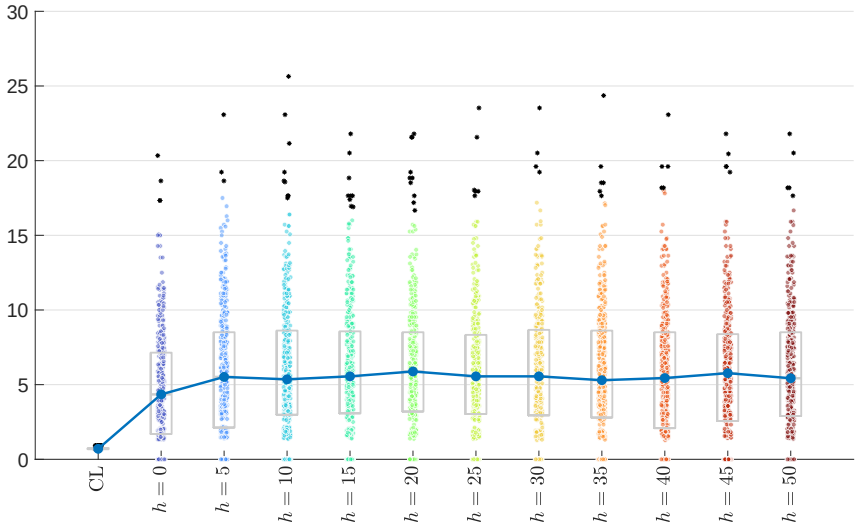

Figure E.1: **Top-1 matching ratios of the freely moving individuals.** Top-1 matching ratios of all 420 pairs (between 21 individuals) are plotted under $h = 0, 5, \cdots, 50$. CL = chance level.

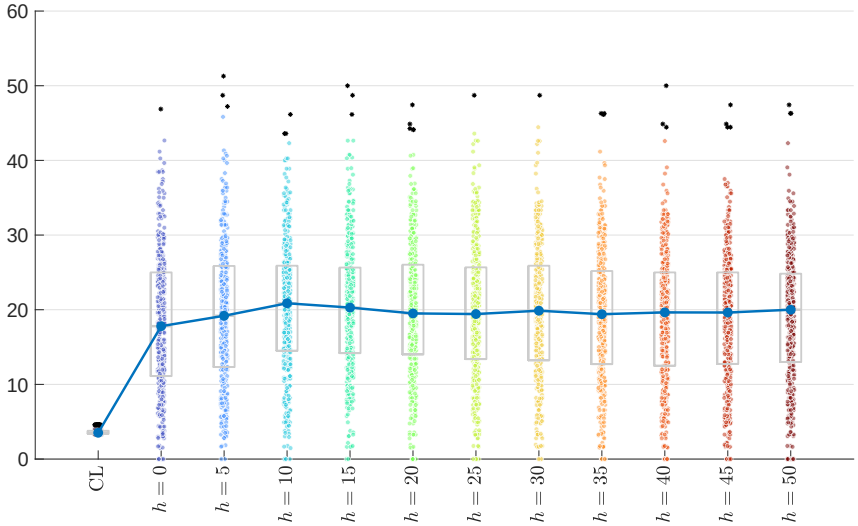

Figure E.2: **Top-5 matching ratios of the freely moving individuals.** Top-5 matching ratios of all 420 pairs plotted under $h = 0, 5, \cdots, 50$. CL = chance level.

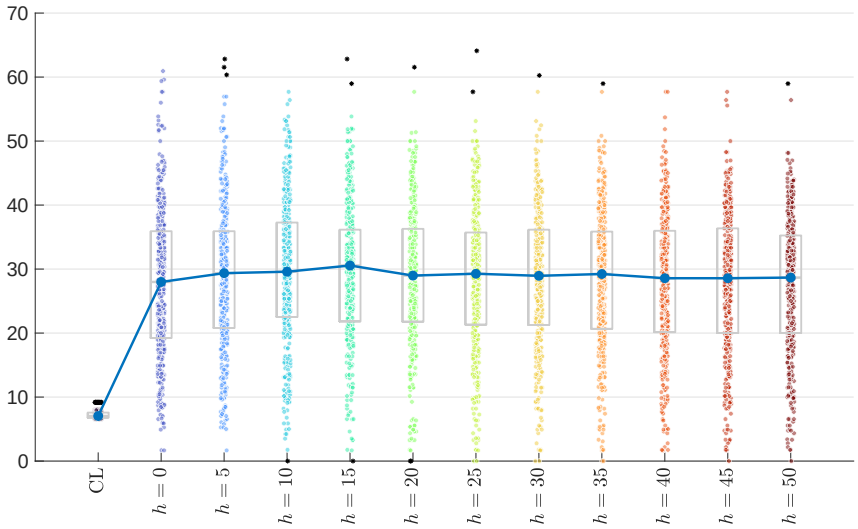

Figure E.3: **Top-10 matching ratios of the freely moving datasets.** Top-10 matching ratios of all 420 pairs plotted under $h = 0, 5, \cdots, 50$. CL = chance level.

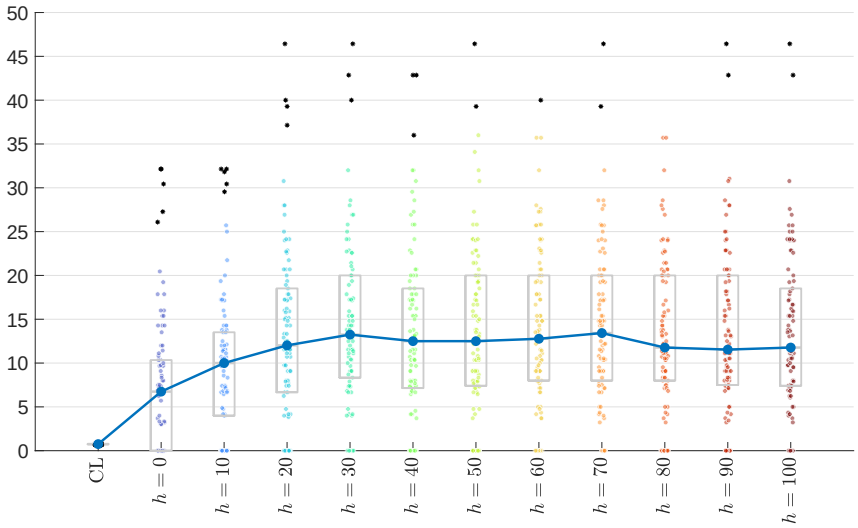

Figure E.4: **Top-1 matching ratios of the immobilized individuals.** Top-1 matching ratios of all 90 pairs (between 10 individuals) plotted under $h = 0, 10, \cdots, 100$. CL = chance level.

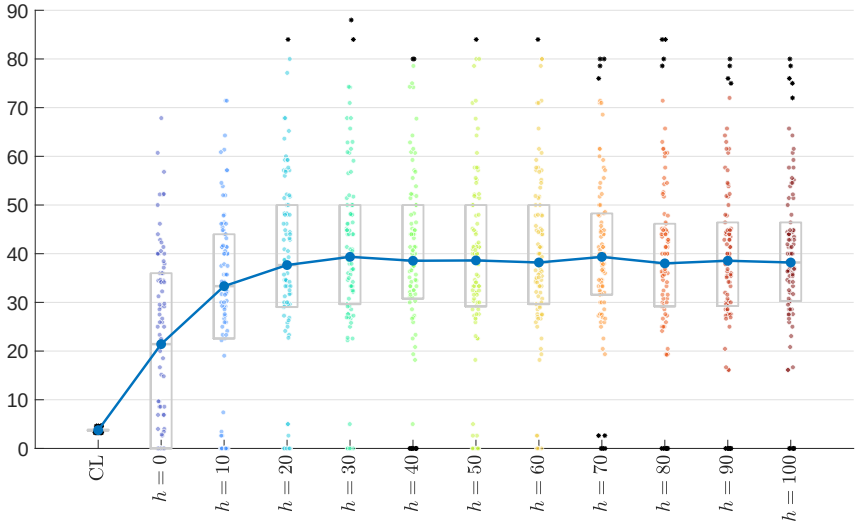

Figure E.5: **Top-5 matching ratios of the immobilized individuals.** Top-5 matching ratios of all 90 pairs under $h = 0, 10, \cdots, 100$. CL = chance level.

We here supplement the matching results under various time delays.

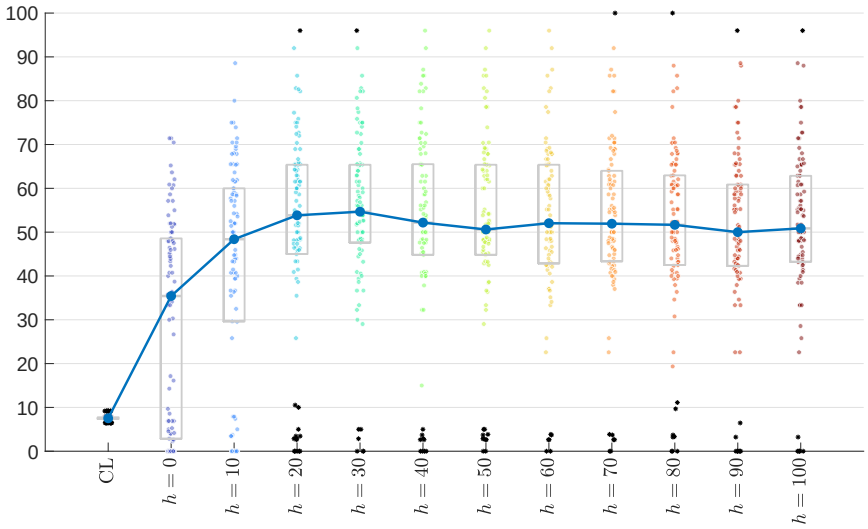

Figure E.6: **Top-10 matching ratios of the immobilized individuals.** Top-10 matching ratios of all 90 pairs plotted under $h = 0, 10, \cdots, 100$. CL = chance level.

F DETAILS OF THE "MAJORITY VOTE"

Prior to the "voting" procedure, we determined the number of individuals whose labels are available to us. We referred to a recent study (Sprague et al., 2024), where the authors trained an automated neuronal identification model with 10 training individuals. To make the comparison between our results and the results in Sprague et al. (2024) reasonable, we first picked out 9 training individuals, whose labels we utilized to identify neuron labels. The number 9 was chosen because it was the closest number we could take out of the 10 immobilized individuals (as explained below, one individual should be left for determining the best time delay, h). The remaining $12\ (= 21 - 9)$ and $1\ (= 10 - 9)$ individuals, in the freely moving or immobilized datasets respectively, are called the test individuals.

We first determined the best hyperparameter for time delay, h, using matching results and the labels of the training individuals. We selected h from $\{0, 5, \cdots, 50\}$ for the freely moving individuals, and from $\{0, 10, \cdots, 100\}$ for the immobilized individuals, so that the time delays in seconds are approximately equal. For each h value, we performed leave-one-out label identification using the training individuals; i.e., we picked one individual from the training set and identified its labels using the labels of the other 8 individuals, and repeated this for all individuals. We then select the value of h that showed the best identification result. Under this h, we tested to what extent we could identify neuron labels of test individuals using the labels of the 9 training individuals.

How did we identify a neuron label with the labels of training individuals based on the matching results? To identify the label of a neuron x in an individual i, we first drew $v(\in \mathbb{N})$ most matched neurons from the matching between i and each of the other individuals. We next examined if the k most frequent neurons in the list of the most matched neurons included the pre-identified label. If the pre-identified label of x is in these k labels, x is called a *correctly elected* label. We then computed the ratio of the correctly elected neurons, using all neuron labels and individuals. See Fig. F.1 for additional explanations.

We randomly took $1,000$ combinations of 9 training individuals out of all 21 freely moving individuals, since the number of all possible combinations is impermissibly large: $\binom{21}{9} \approx 300,000$. We took all $10\ (= \binom{10}{9})$ combinations of 9 individuals out of all 10 immobilized individuals.

We counted for each individual the numbers of correctly elected labels and calculated the percentages of them. Under $v = 5$ and $k = 5$, the ratio of correctly elected neurons was 46% in the freely moving individuals. The ratio was even larger in the immobilized individuals, hitting as high as 56%. These rather large values demonstrate the efficacy of our framework. We here presented results under $v = 5$ and $k = 5$ as an example, but changing $v = 10$ yielded similar results. We show the results under $v = 1, 5, 10$ and $k = 1, 3, 5$ in Appendix Figs F.2 and F.3.

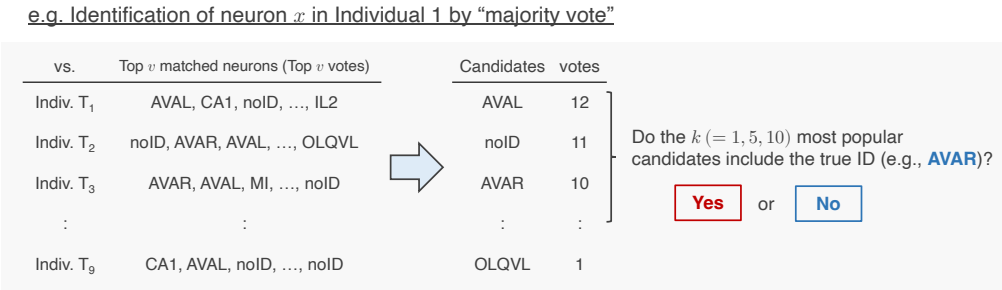

Figure F.1: **"The majority vote".** This figure describes the identification process by the "majority vote" for a neuron named x of an individual (called Individual 1) as an example. x has its pre-identified neuron label (e.g., "AVAR") but we do not use this information at this point. To identify x, we take nine individuals $\{T_1, \cdots, T_9\}$, whose labels are available. Below we provide a step-by-step explanation. Step 1) We take the v-largest neurons from each of the matching matrices between Individual 1 and the nine individuals, or, we let the nine individuals cast v "votes" for the possible labels of x (leftmost table). v is a predetermined integer, which we set in this work $v = 1, 5, 10$. Step 2) We sum up how many times a label appeared in the table and arrange them in descending order, which yields a list of candidate labels for x (middle table). This list can include neurons without labels, denoted by "noID" in the figure. Step 3) We take the k-largest appearing candidates from the list and check if these candidates include the pre-identified label. We excluded "noID" from the k-largest candidates. If the k-largest candidates include the labels with zero votes, we excluded that label as well from the candidates. In this example, the pre-identified label, "AVAR", is the third candidate. Hence this neuron is *correctly elected* under $k = 5$ or more, but is not under $k = 1$. Step 4) We performed the same procedure for all labeled neurons in an individual and computed the percentage of the correctly elected neurons. We then carried out this procedure with all individuals in the dataset.

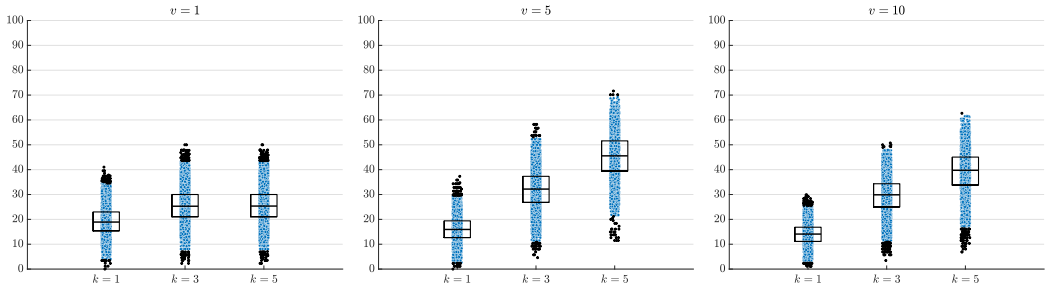

Figure F.2: **Percentages of "correctly elected" neurons in the majority vote procedure under various v and k values in the freely moving individuals.**

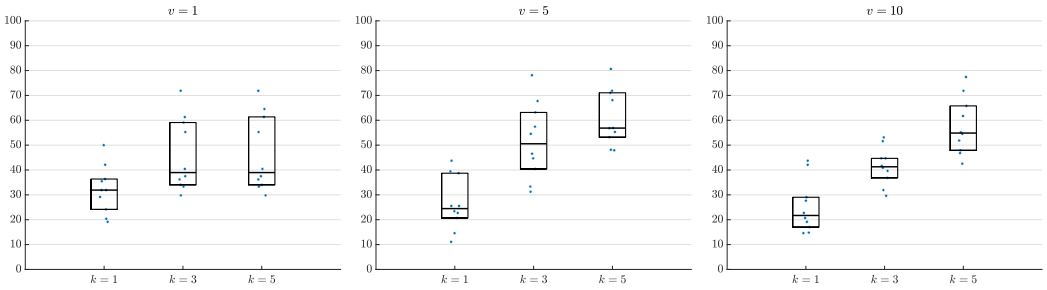

Figure F.3: **Percentages of "correctly elected" neurons in the majority vote procedure under various v and k values in the immobilized individuals.**